Monte Carlo Analysis of the Ising Model: From π estimation to critical behaviour in one and two dimensions

Yash Singh Bedi YXB337

December 2025

Abstract

Monte Carlo methods are applied to a sequence of problems of increasing complexity. As a warm up, simple Monte Carlo integration is used to estimate π from random points in a square and the resulting distribution of estimates is compared with the central limit theorem, providing a quantitative test of the statistical error analysis. The Ising model is then simulated in one and two dimensions with single-spin Metropolis updates and, near criticality, parallel tempering. For the one-dimensional chain the Monte Carlo energy per spin agrees with the exact thermodynamic-limit result within statistical errors. For the two-dimensional ferromagnetic model on $L \times L$ lattices with $L = 16$–64, energy, magnetisation, specific heat, susceptibility and Binder cumulants are measured. Finite-size scaling of the susceptibility peaks gives $\gamma/\nu = 1.80 \pm 0.18$, compatible with the exact value $7/4$, while the specific-heat peaks are consistent with the logarithmic growth implied by $\alpha = 0$. From the shift of the susceptibility peaks we estimate $T_c(\infty) = 2.243 \pm 0.022$, in agreement with the Onsager critical temperature. The antiferromagnetic Ising model is also studied: on a 16×16 lattice the staggered magnetisation remains close to 1 at low temperature and drops rapidly around $T \approx 2.3$ while the uniform magnetisation stays near zero. A limited antiferromagnetic finite-size scaling study of the staggered susceptibility for $L = 16, 24, 32$ gives noisy but compatible estimates of γ/ν and T_c. For the lattice sizes considered, integrated autocorrelation times show that parallel tempering reduces the variance of the mean-energy estimator by only about 10–15% compared with a single Metropolis chain of equal length.

1 Introduction

The Ising model is a standard example in statistical mechanics and critical phenomena. In two dimensions it exhibits a continuous phase transition with exactly known critical temperature and exponents [1, 2], making it an ideal test bed for Monte Carlo algorithms and finite-size scaling (FSS) techniques [5, 3, 4].

The aims of this project are:

- to introduce Monte Carlo integration via an estimate of π and comparison with the central limit theorem;
- to validate a Metropolis implementation of the Ising model by comparing one-dimensional Monte Carlo results with exact analytics;
- to measure thermodynamic observables of the two-dimensional ferromagnetic Ising model near criticality for several lattice sizes and to extract γ/ν, an effective α/ν, and an estimate of the infinite-volume critical temperature T_c;
- to study the temperature dependence of energy and order parameters in the two-dimensional antiferromagnetic Ising model on a 16×16 lattice and perform a small finite-size scaling analysis of the staggered susceptibility for $L = 16, 24, 32$ as a universality cross-check;

- to quantify any efficiency gain from parallel tempering relative to a single Metropolis chain using autocorrelation-based error analysis.

Section 2 describes the π warm up. Section 3 defines the Ising model, observables and algorithms. Section 4 presents the one-dimensional validation. Section 5 discusses single-size behaviour in two dimensions, including the antiferromagnetic model. Section 6 contains the finite-size scaling analysis and the antiferromagnetic cross-check. Section 7 compares parallel tempering with Metropolis. Section 8 summarises the main results.

Unless stated otherwise, uncertainties are one-sigma statistical errors from autocorrelation-aware estimators or weighted least-squares fits. For some shorter scans (in particular the antiferromagnetic finite-size analysis) a simple blocking estimator is used; on a subset of data this was checked to agree with the autocorrelation-based errors within uncertainties.

2 Monte Carlo estimation of π

2.1 Method

To illustrate Monte Carlo integration, the area of a unit circle is estimated. Consider the square $[-1,1]\times[-1,1]$ of area $A_{\text{square}}=4$, inside which the unit circle of area $A_{\text{circle}}=\pi$ is inscribed. If (x,y) is drawn uniformly from the square then the indicator

$$I(x,y)=\begin{cases}1, & x^2+y^2\le 1,\\ 0, & x^2+y^2>1\end{cases} \tag{1}$$

has expectation

$$\mathbb{E}[I]=\frac{A_{\text{circle}}}{A_{\text{square}}}=\frac{\pi}{4}. \tag{2}$$

Drawing N independent points (x_i,y_i) and forming

$$\hat{p}=\frac{1}{N}\sum_{i=1}^{N} I(x_i,y_i), \tag{3}$$

gives the estimator

$$\hat{\pi}=4\hat{p}. \tag{4}$$

The variance of $\hat{\pi}$ for a single run is

$$\operatorname{Var}(\hat{\pi})=16\,\operatorname{Var}(\hat{p})=\frac{16}{N}p(1-p),\qquad p=\frac{\pi}{4}, \tag{5}$$

so the predicted standard deviation is

$$\sigma_{\hat{\pi}}^{(\text{CLT})}=\sqrt{\frac{16}{N}p(1-p)}. \tag{6}$$

For large N the central limit theorem predicts that the distribution of $\hat{\pi}$ from independent runs is approximately normal with this variance.

2.2 Results

To test both the Monte Carlo implementation and the error formula, $N_{\text{runs}}=1000$ independent runs were performed, each with $N=10000$ samples. For each run r the estimator $\hat{\pi}_r$ was recorded. From these data

$$\overline{\hat{\pi}}=3.141916, \tag{7}$$

$$s_{\hat{\pi}}=0.016514, \tag{8}$$

$$s_{\overline{\hat{\pi}}}=0.000522. \tag{9}$$

The true value is $\pi = 3.141593$, so the bias

$$\overline{\hat{\pi}} - \pi = 3.23 \times 10^{-4} \tag{10}$$

is far smaller than $s_{\overline{\hat{\pi}}}$.

From the analytic formula with $N = 10000$ the predicted standard deviation is

$$\sigma_{\hat{\pi}}^{(\mathrm{CLT})} = 0.016422, \tag{11}$$

in excellent agreement with $s_{\hat{\pi}}$.

Figure 1 shows the histogram of the 1000 values of $\hat{\pi}$ together with a normal distribution with mean $\overline{\hat{\pi}}$ and standard deviation $s_{\hat{\pi}}$. The data follow the Gaussian closely and are centred near the true π, validating both the estimator and the CLT-based error estimate.

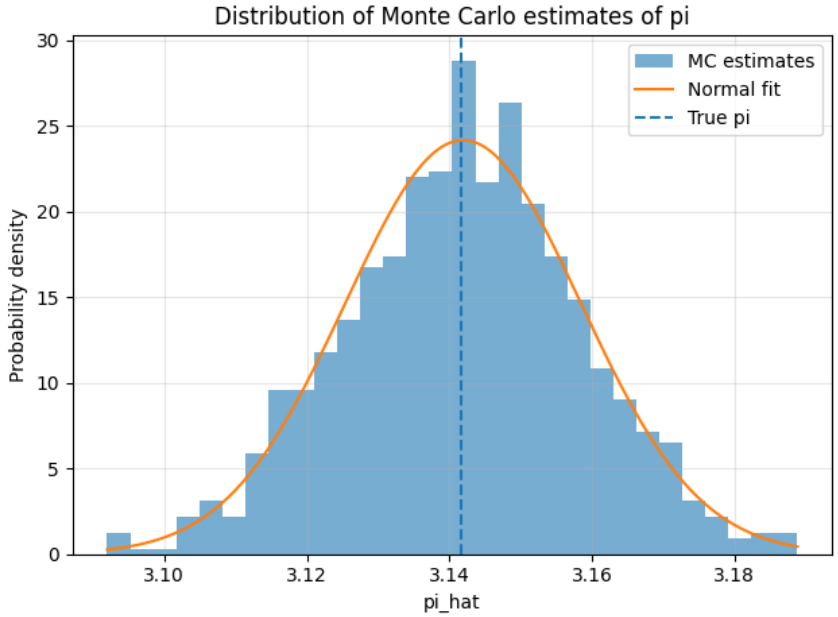

Figure 1: Distribution of Monte Carlo estimates of π from 1000 runs with $N = 10000$ samples each. The solid line is a normal fit with the measured mean and standard deviation; the vertical dashed line marks the true value of π.

3 Model, observables and algorithms

3.1 Ising Hamiltonian

On a square lattice of size $L \times L$ with periodic boundaries the Ising Hamiltonian is

$$H(\{s_i\}) = -J \sum_{\langle ij \rangle} s_i s_j, \tag{12}$$

with spins $s_i = \pm 1$ and nearest-neighbour coupling J. For the ferromagnet $J > 0$ and neighbouring spins prefer to align, while for the antiferromagnet $J < 0$ and neighbours prefer to be opposite. In what follows $|J| = 1$ and $k_B = 1$.

The energy per spin is $e = H/N$ with $N = L^2$. For the ferromagnet the magnetisation per spin is

$$m = \frac{1}{N} \sum_i s_i, \tag{13}$$

and the order parameter used in plots is the average absolute magnetisation $\langle |m| \rangle$. For the antiferromagnet it is convenient to define the staggered magnetisation

$$m_s = \frac{1}{N} \sum_i \epsilon_i s_i, \tag{14}$$

where $\epsilon_i = (-1)^{x_i + y_i}$ for a site at (x_i, y_i). In the perfectly ordered Néel state, $|m_s| = 1$ and $m = 0$.

The thermal averages used later are

$$\langle e \rangle, \qquad \langle |m| \rangle, \qquad \langle |m_s| \rangle, \qquad C_v = \frac{N}{T^2} \left(\langle e^2 \rangle - \langle e \rangle^2 \right), \tag{15}$$

$$\chi = \frac{N}{T} \left(\langle m^2 \rangle - \langle m \rangle^2 \right), \tag{16}$$

and the Binder cumulant

$$U_4 = 1 - \frac{\langle m^4 \rangle}{3 \langle m^2 \rangle^2}. \tag{17}$$

In a finite system with symmetric dynamics and zero field, $\langle m \rangle$ is close to zero at all temperatures, so in practice $\chi \approx (N/T) \langle m^2 \rangle$. The absolute value $\langle |m| \rangle$ is used as a convenient order parameter in plots.

Near the ferromagnetic critical point these quantities scale with L as [5]

$$C_{v,\max}(L) \sim L^{\alpha/\nu}, \tag{18}$$

$$\chi_{\max}(L) \sim L^{\gamma/\nu}, \tag{19}$$

$$T_c(L) - T_c(\infty) \sim L^{-1/\nu}, \tag{20}$$

and for the two-dimensional ferromagnet the exact exponents are $\nu = 1$, $\alpha = 0$ (logarithmic divergence), $\beta = 1/8$, $\gamma = 7/4$ [2].

3.2 Metropolis updates

All local sampling was done using the single-spin Metropolis algorithm [3, 4]. For each attempted flip at site i, the energy change $\Delta E = 2 J s_i \sum_{j \in \text{n.n.}(i)} s_j$ was computed and accepted with probability

$$p_{\text{acc}} = \begin{cases} 1, & \Delta E \le 0, \\ e^{-\beta \Delta E}, & \Delta E > 0, \end{cases} \tag{21}$$

with $\beta = 1/T$. One sweep corresponds to N such updates with sites chosen uniformly at random.

The update used in the simulations is summarised in Algorithm 1.

3.3 Parallel tempering

Parallel tempering (PT) runs several replicas of the system at different temperatures T_k in parallel [4]. Each replica performs Metropolis sweeps at its own temperature. After a fixed number of sweeps, neighbouring replicas k and $k+1$ attempt to swap configurations with acceptance probability

$$p_{\text{swap}} = \min\left(1, \exp\left[(\beta_k - \beta_{k+1})(E_{k+1} - E_k)\right]\right). \tag{22}$$

This leaves the joint distribution invariant but allows configurations to diffuse in temperature space, which can reduce trapping in metastable states.

In this project a ladder of $R = 8$ temperatures was used between $T_{\min} = 1.8$ and $T_{\max} = 3.0$ for both $L = 16$ and $L = 24$. Swap attempts were made every ten sweeps. The observed swap acceptance rates were about 0.46 for $L = 16$ and 0.28 for $L = 24$.

Algorithm 1 Single-spin Metropolis sweep for the 2D Ising model

Require: Spin configuration $s_{i,j} = \pm 1$ on an $L \times L$ lattice, inverse temperature β, number of sweeps N_{sweeps}.

for $s = 1$ to N_{sweeps} **do**
  for $n = 1$ to L^2 **do**
    Choose a random site (i, j).
    Compute neighbour sum $S = s_{i-1,j} + s_{i+1,j} + s_{i,j-1} + s_{i,j+1}$ with periodic boundaries.
    Compute energy change $\Delta E = 2 J s_{i,j} S$.
    if $\Delta E \leq 0$ **then**
      Flip spin: $s_{i,j} \leftarrow -s_{i,j}$.
    else
      Draw $u \sim U(0, 1)$.
      if $u < e^{-\beta \Delta E}$ **then**
        Flip spin: $s_{i,j} \leftarrow -s_{i,j}$.
      end if
    end if
  end for
end for

3.4 Error estimation and autocorrelations

Monte Carlo samples are correlated in simulation time. For a time series x_t (energy or magnetisation) the normalised autocorrelation function $\rho(\tau)$ and the integrated autocorrelation time τ_{int} were estimated as

$$\rho(\tau) = \frac{\langle (x_t - \bar{x})(x_{t+\tau} - \bar{x}) \rangle}{\langle (x_t - \bar{x})^2 \rangle}, \tag{23}$$

$$\tau_{\text{int}} = \tfrac{1}{2} + \sum_{\tau=1}^{\tau_{\max}} \rho(\tau), \tag{24}$$

where the sum was cut once $\rho(\tau)$ first became non-positive.

The effective number of independent measurements is

$$N_{\text{eff}} = \frac{N_{\text{samples}}}{2 \tau_{\text{int}}}, \tag{25}$$

and the standard error on the mean is

$$\sigma_{\bar{x}} = \sqrt{\frac{\sigma_x^2}{N_{\text{eff}}}}, \tag{26}$$

with σ_x^2 the sample variance.

The automatic estimation of τ_{int} and $\sigma_{\bar{x}}$ follows Algorithm 2.

For the large-scale 2D runs used in the FSS analysis, typical integrated autocorrelation times for the energy and magnetisation in the temperature window $T \in [1.8, 3.0]$ were of order unity in units of recorded measurements, giving effective sample sizes of several hundred to about a thousand per (L, T).

For some shorter scans (for example the AFM finite-size study in Sec. 6.6) a simple blocking analysis of the time series was used instead of an explicit autocorrelation sum; on representative segments of the ferromagnetic data the blocking and τ_{int} methods agree within the quoted errors.

Algorithm 2 Autocorrelation and error estimation for a time series

Require: Time series x_t of length N, maximum lag $\tau_{\max}$.
Compute mean $\bar{x} = \frac{1}{N}\sum_{t=1}^{N} x_t$.
Form centred series $y_t = x_t - \bar{x}$.
Compute variance $\sigma_x^2 = \frac{1}{N}\sum_{t=1}^{N} y_t^2$.
Set $\rho(0) = 1$.
for $\tau = 1$ to $\tau_{\max}$ **do**
  Compute $\rho(\tau) = \frac{1}{(N-\tau)\sigma_x^2}\sum_{t=1}^{N-\tau} y_t\, y_{t+\tau}$.
end for
Set $\tau_{\text{int}} \leftarrow \frac{1}{2}$.
for $\tau = 1$ to $\tau_{\max}$ **do**
  if $\rho(\tau) \le 0$ **then**
    break
  end if
  $\tau_{\text{int}} \leftarrow \tau_{\text{int}} + \rho(\tau)$.
end for
Compute $N_{\text{eff}} = N/(2\tau_{\text{int}})$.
Compute standard error $\sigma_{\bar{x}} = \sqrt{\sigma_x^2/N_{\text{eff}}}$.
return $\tau_{\text{int}}, N_{\text{eff}}, \sigma_{\bar{x}}$.

4 Validation in one dimension

A one-dimensional Ising chain with $N = 64$ spins over $T \in [0.01, 4]$ was used to check the implementation and statistical analysis. The exact energy per spin for the infinite chain is

$$e_{\text{exact}}(T) = -\tanh(\beta J), \tag{27}$$

which follows from the transfer-matrix solution [2].

Figure 2 compares the Monte Carlo estimate with the analytic thermodynamic-limit curve. For this chain length the Monte Carlo data track the exact result closely: deviations are at the level of the statistical error bars for $T \gtrsim 0.5$, and only at the very lowest temperatures do small finite-size effects become visible. The limits $e \to 0$ at high T and $e \to -1$ as $T \to 0$ are reproduced.

The average absolute magnetisation per spin (Fig. 3) smoothly decreases with T, reflecting the absence of a phase transition in one dimension with short-range interactions.

These tests provide a basic but stringent check of the Metropolis update and observable routines on a model with known analytic behaviour.

5 Single-size behaviour in two dimensions

5.1 Antiferromagnetic model on $L = 16$

The two-dimensional antiferromagnetic Ising model was simulated with $J = -1$ on a 16×16 lattice. Both the uniform magnetisation $|m|$ and the staggered magnetisation $|m_s|$ were measured.

A temperature sweep over $T \in [0.01, 4.0]$ was performed. For each temperature the simulation used 1000 burn-in sweeps followed by 5000 measurement sweeps, recording every tenth sweep. Table 1 summarises the resulting estimates of the energy per spin and the two order parameters.

The corresponding curves are plotted in Fig. 4. At low temperature the energy per spin is -2, corresponding to a Néel ordered state with $\langle |m_s| \rangle \approx 1$ and negligible uniform magnetisation.

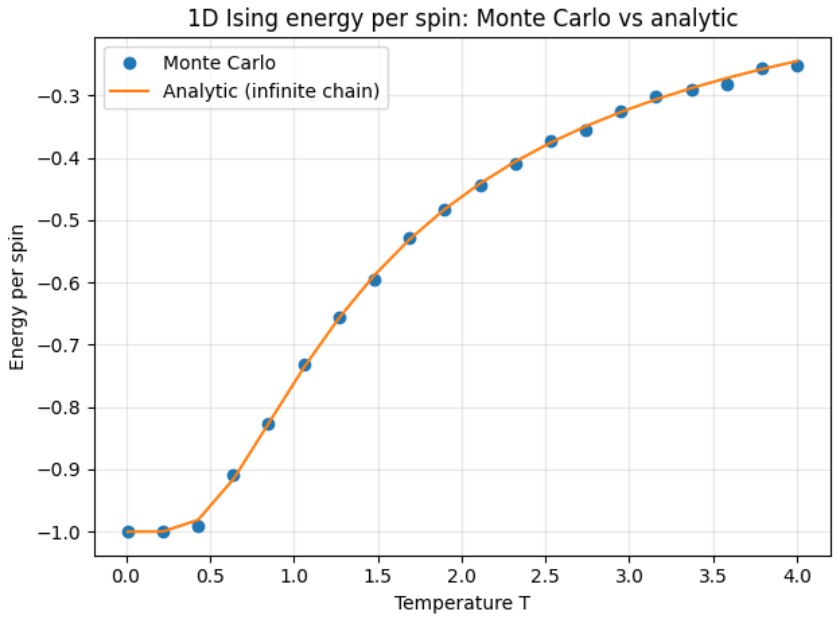

Figure 2: Energy per spin in the 1D Ising model: Monte Carlo data (symbols) and exact thermodynamic-limit result (line).

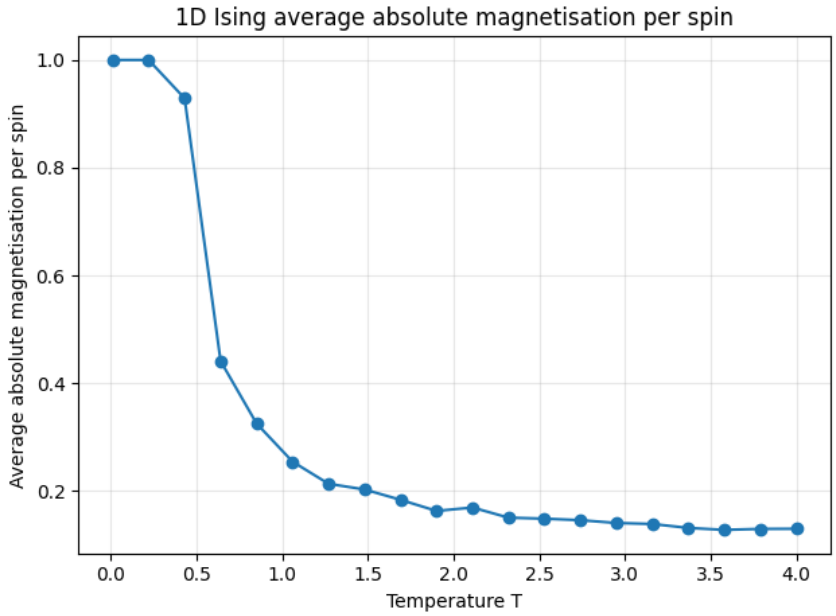

Figure 3: Average absolute magnetisation per spin for the 1D chain as a function of temperature.

Table 1: Thermodynamic observables for the 2D antiferromagnetic Ising model on an $L = 16$ lattice.

T	$\langle E \rangle / N$	$\langle \lvert m \rvert \rangle$	$\langle \lvert m_s \rvert \rangle$
0.010	-2.0000 ± 0.0000	0.0000 ± 0.0000	1.0000 ± 0.0000
0.220	-2.0000 ± 0.0000	0.0000 ± 0.0000	1.0000 ± 0.0000
0.430	-2.0000 ± 0.0000	0.0000 ± 0.0000	1.0000 ± 0.0000
0.640	-2.0000 ± 0.0000	0.0000 ± 0.0000	1.0000 ± 0.0000
0.850	-1.9993 ± 0.0001	0.0002 ± 0.0000	0.9998 ± 0.0000
1.060	-1.9953 ± 0.0007	0.0010 ± 0.0001	0.9988 ± 0.0002
1.270	-1.9826 ± 0.0011	0.0030 ± 0.0003	0.9954 ± 0.0003
1.480	-1.9550 ± 0.0007	0.0060 ± 0.0002	0.9876 ± 0.0002
1.690	-1.9021 ± 0.0020	0.0090 ± 0.0003	0.9716 ± 0.0008
1.900	-1.8091 ± 0.0003	0.0121 ± 0.0002	0.9383 ± 0.0010
2.110	-1.6567 ± 0.0034	0.0161 ± 0.0003	0.8694 ± 0.0019
2.320	-1.3698 ± 0.0294	0.0204 ± 0.0004	0.6291 ± 0.0583
2.530	-1.1033 ± 0.0038	0.0242 ± 0.0004	0.3668 ± 0.0083
2.740	-0.9422 ± 0.0049	0.0261 ± 0.0005	0.2257 ± 0.0143
2.950	-0.8394 ± 0.0045	0.0274 ± 0.0010	0.1788 ± 0.0036
3.160	-0.7563 ± 0.0055	0.0284 ± 0.0002	0.1484 ± 0.0054
3.370	-0.6956 ± 0.0041	0.0290 ± 0.0002	0.1334 ± 0.0017
3.580	-0.6431 ± 0.0041	0.0301 ± 0.0006	0.1181 ± 0.0027
3.790	-0.5962 ± 0.0017	0.0325 ± 0.0006	0.1092 ± 0.0019
4.000	-0.5570 ± 0.0022	0.0329 ± 0.0004	0.1017 ± 0.0025

Around $T \approx 2.3$ the energy rises rapidly and $\langle \lvert m_s \rvert \rangle$ drops from values close to one to around 0.4 and then 0.2 by $T \approx 2.7$, signalling the loss of long-range antiferromagnetic order. Across the whole temperature range $\langle \lvert m \rvert \rangle$ remains small, never exceeding about 0.033, consistent with symmetry between the two Néel ground states.

These results show that the antiferromagnetic couplings and staggered order parameter are implemented correctly in the code.

5.2 Ferromagnetic case at fixed L

A similar temperature sweep was performed for the ferromagnetic model at $L = 16$. The energy, magnetisation, specific heat and susceptibility show the expected behaviour: $e \to -2$ and $\lvert m \rvert \to 1$ at low T, and a rapid crossover to $e \approx 0$ and small $\lvert m \rvert$ near $T \approx 2.3$. These scans were used to choose the temperature window for the finite-size scaling analysis.

6 Finite-size scaling and critical behaviour

6.1 Simulation set-up

For the scaling analysis, lattice sizes $L = 16, 24, 32, 40, 48, 56, 64$ were simulated at 24 temperatures between $T = 1.8$ and $T = 3.0$. Each run used

- $N_{\mathrm{burn}} = 4000$ Metropolis sweeps for equilibration,
- $N_{\mathrm{meas}} = 12000$ sweeps with measurements every 10 sweeps,
- roughly 1200 recorded configurations per (L, T).

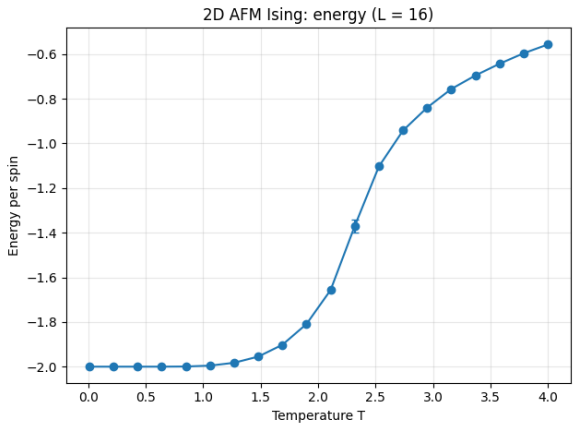

(a) Energy per spin.

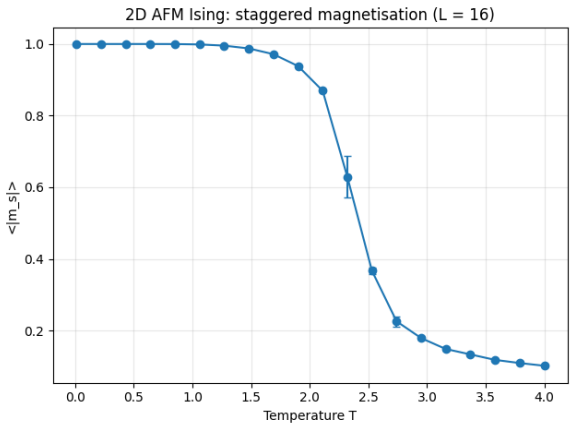

(b) Average absolute staggered magnetisation.

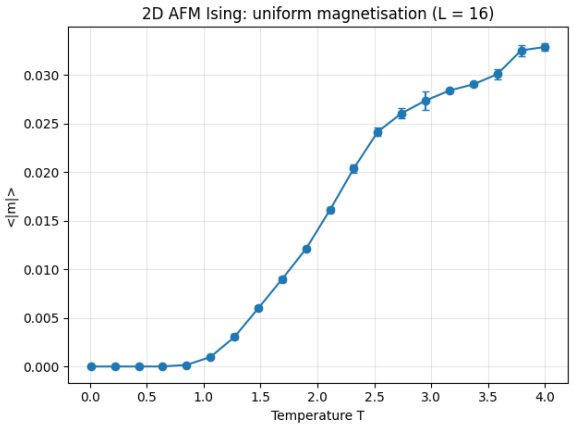

(c) Average absolute uniform magnetisation.

Figure 4: Thermodynamic observables for the 2D antiferromagnetic Ising model on an $L = 16$ lattice.

Binder cumulants, specific heat and susceptibility were computed from these samples along with their statistical errors.

6.2 Binder cumulants

Figure 5 shows the Binder cumulant $U_4(T, L)$ for all seven lattice sizes. At low T all curves sit near $U_4 \approx 2/3$. Around $T \approx 2.25$ they begin to separate and cross in a narrow window, with crossings compatible with the known critical temperature $T_c \approx 2.269$. Here the Binder cumulant is used mainly as a qualitative consistency check.

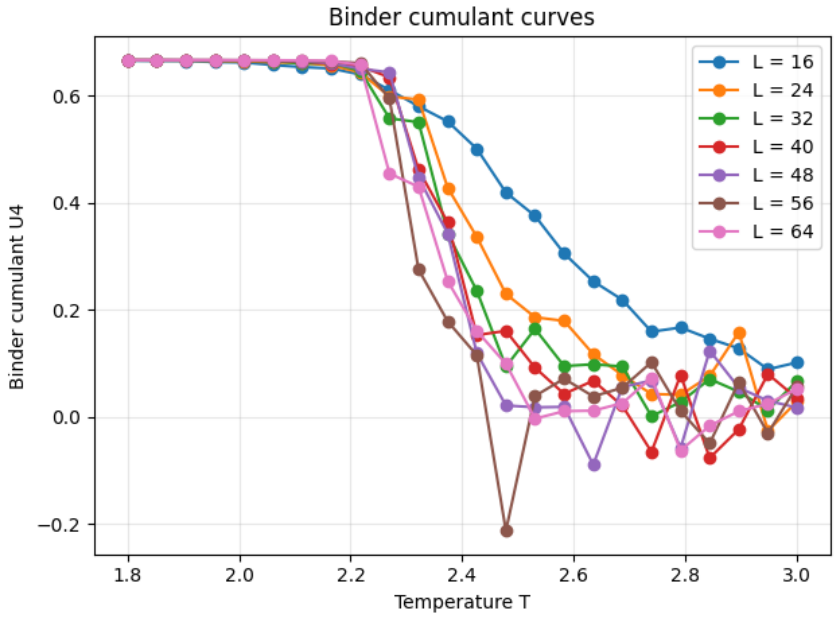

Figure 5: Binder cumulant U_4 as a function of temperature for several lattice sizes in the 2D ferromagnetic Ising model.

6.3 Peak heights and exponent ratios

For each lattice size, the maxima of $C_v(T)$ and $\chi(T)$ on the simulated temperature grid were identified. The maximum specific heats were fitted to Eq. (18),

$$C_{v,\max}(L) = a_C L^{\alpha/\nu}, \tag{28}$$

in log–log space using the statistical errors as weights. The fit gave

$$\alpha/\nu = 0.090 \pm 0.030, \qquad \chi^2/\mathrm{dof} = 2.7. \tag{29}$$

The fitted exponent is small and positive, but the error bar and slightly elevated χ^2/dof suggest that a pure power law is not optimal. Since theory predicts $\alpha = 0$ and a logarithmic divergence [2], an alternative fit

$$C_{v,\max}(L) = a_0 + b \log L \tag{30}$$

was performed, giving

$$b = 0.155 \pm 0.048, \qquad \chi^2/\mathrm{dof} = 2.1. \tag{31}$$

The roughly linear trend in Fig. 7 supports a logarithmic growth of $C_{v,\max}(L)$.

For the susceptibility peaks a power-law fit to Eq. (19),

$$\chi_{\max}(L) = a_\chi L^{\gamma/\nu}, \tag{32}$$

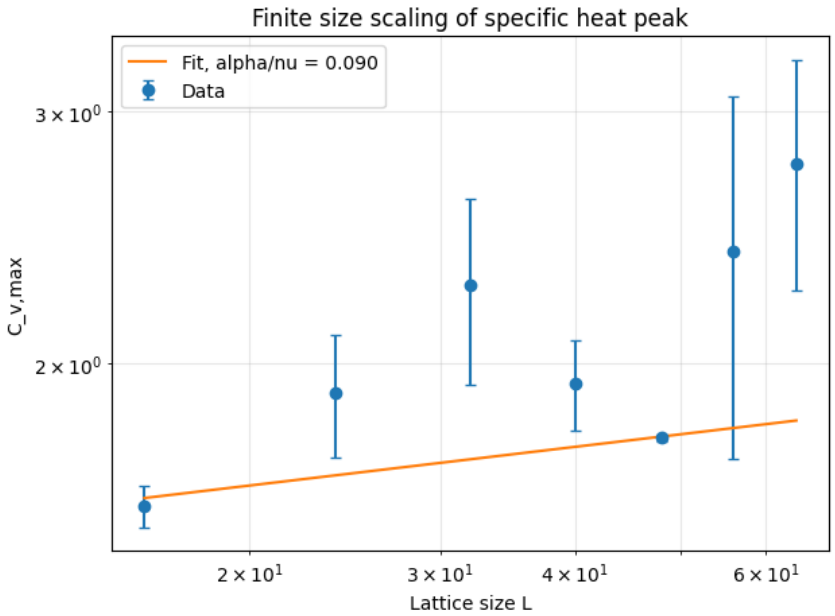

Figure 6: Finite-size scaling of the specific-heat peak for the 2D ferromagnetic Ising model.

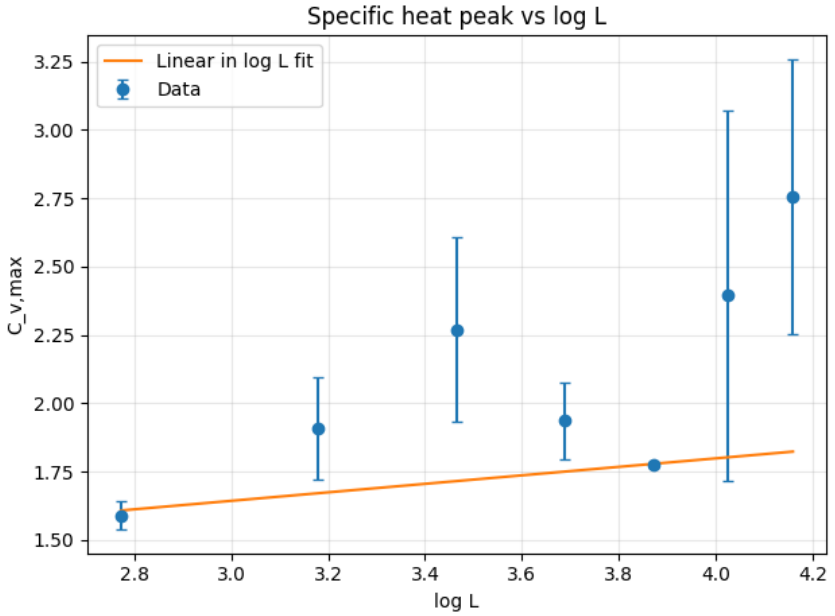

Figure 7: Specific-heat peak as a function of $\log L$ with a linear fit, consistent with a logarithmic divergence.

gave

$$\gamma/\nu = 1.80 \pm 0.18, \qquad \chi^2/\mathrm{dof} = 0.02. \tag{33}$$

Within errors this matches the exact value $\gamma/\nu = 7/4$. The error bar should be interpreted as a lower bound, since systematic effects from the temperature grid and limited size range are comparable to the fit error.

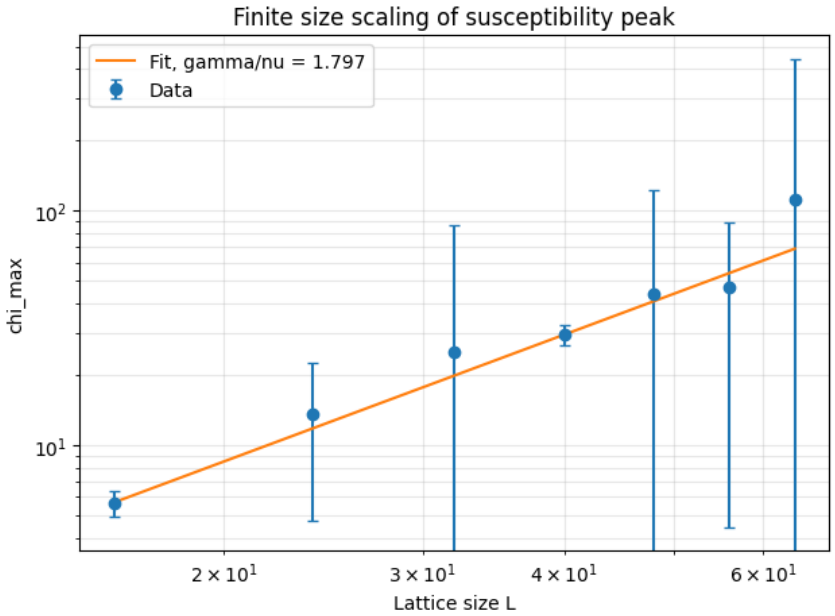

Figure 8: Finite-size scaling of the susceptibility peak with power-law fit.

6.4 Pseudocritical temperatures and T_c

Let $T_c^*(L)$ denote the temperature at which $\chi(T, L)$ reaches its maximum. Assuming $\nu = 1$, a weighted linear fit in $1/L$ to Eq. (20),

$$T_c^*(L) = T_c + aL^{-1}, \tag{34}$$

yields

$$T_c(\infty) = 2.243 \pm 0.022, \qquad \chi^2/\mathrm{dof} = 1.6. \tag{35}$$

This is consistent with the exact result $T_c = 2/\ln\bigl(1+\sqrt{2}\bigr) \approx 2.269$ [1, 2]. The dominant uncertainties arise from the coarse temperature grid and noise in χ for the largest lattices.

6.5 Susceptibility data collapse

A simple scaling test is obtained by plotting

$$\chi(L,T)L^{-\gamma/\nu} \quad \text{against} \quad (T - T_c)L^{1/\nu}. \tag{36}$$

Using $\gamma/\nu = 1.80$, $\nu = 1$, and $T_c = 2.243$, all susceptibility data in $1.8 \le T \le 3.0$ were rescaled according to Eq. (36). The resulting curves for different L fall on a common peak with only mild spread (Fig. 9), indicating a satisfactory data collapse.

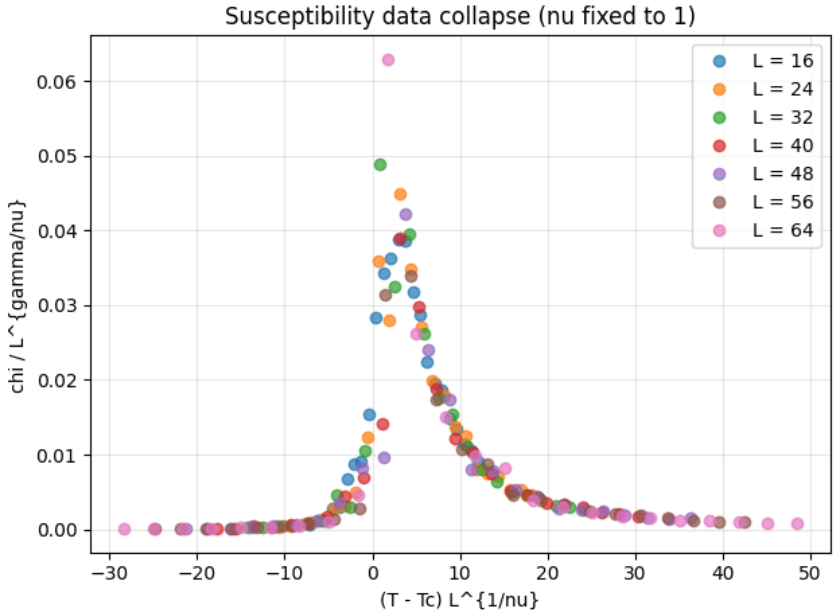

Figure 9: Scaling collapse of the susceptibility using $\gamma/\nu = 1.80$, $\nu = 1$, and $T_c = 2.243$ for the 2D ferromagnetic Ising model.

6.6 Antiferromagnetic finite-size scaling cross-check

To check explicitly that the antiferromagnetic model lies in the same universality class, a reduced finite-size analysis was performed using the staggered order parameter. Simulations with $J = -1$ were run for $L = 16, 24, 32$ on the same temperature grid $T \in [1.8, 3.0]$ with 4000 burn-in sweeps, 12000 measurement sweeps and sampling every 10 sweeps. For each (L, T) the energy, staggered magnetisation m_s and

$$C_v(T, L) = \frac{N}{T^2}\left(\langle e^2\rangle - \langle e\rangle^2\right), \qquad \chi_s(T, L) = \frac{N}{T}\left(\langle m_s^2\rangle - \langle m_s\rangle^2\right) \tag{37}$$

were estimated using a blocking analysis. In practice $\langle m_s\rangle$ is statistically consistent with zero, so $\chi_s \approx (N/T)\langle m_s^2\rangle$. The staggered susceptibility exhibits a clear peak for each lattice size, with peak height increasing and the pseudocritical temperature shifting towards lower T as L grows.

The pseudocritical temperatures from the maxima of $\chi_s(T, L)$ are approximately

$$T_c^{*,\mathrm{AFM}}(16) \approx 2.426, \qquad T_c^{*,\mathrm{AFM}}(24) \approx 2.322, \qquad T_c^{*,\mathrm{AFM}}(32) \approx 2.322, \tag{38}$$

with corresponding peak heights

$$\chi_{s,\max}(16) \approx 5.99, \quad \chi_{s,\max}(24) \approx 12.7, \quad \chi_{s,\max}(32) \approx 20.9. \tag{39}$$

A log–log fit of

$$\chi_{s,\max}(L) = a_s L^{\gamma/\nu} \tag{40}$$

(Fig. 10) yields

$$\gamma/\nu_{\mathrm{AFM}} = 1.809 \pm 1.485, \tag{41}$$

consistent with both the ferromagnetic estimate and the exact value $7/4$, though with large errors.

Assuming $\nu = 1$, a fit of

$$T_c^{*,\mathrm{AFM}}(L) = T_c^{\mathrm{AFM}} + \frac{a}{L}, \tag{42}$$

treating half the temperature grid spacing as an error, gives

$$T_c^{\mathrm{AFM}}(\infty) = 2.195 \pm 0.054, \tag{43}$$

compatible with $T_c(\infty)$ from the ferromagnetic analysis and the exact Onsager result. Given the small number of lattice sizes and sizeable statistical errors, this AFM study is best viewed as a qualitative universality check rather than a precision determination.

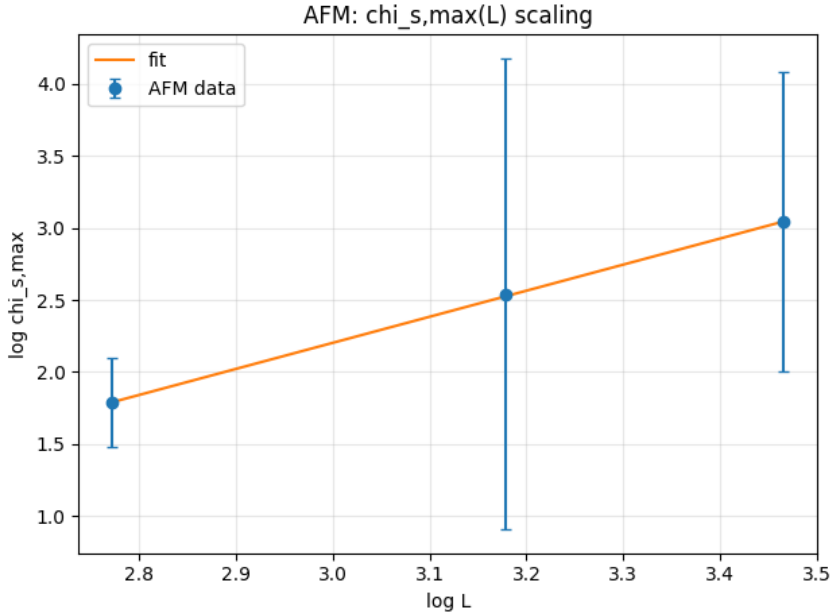

Figure 10: Finite-size scaling of the maximum staggered susceptibility $\chi_{s,\max}(L)$ for the antiferromagnetic Ising model.

6.7 Correlation length at $T = 2.3$

To connect with the real-space picture of criticality, the spin-spin correlation function

$$C(r) = \langle s_i s_{i+r} \rangle - \langle s_i \rangle^2 \tag{44}$$

was estimated for $L = 32$ at $T = 2.3$, slightly above the best-fit critical temperature. After a burn-in of 10000 sweeps, 1000 configurations were sampled every 50 sweeps. Correlations along one lattice axis were averaged over all sites and configurations.

For distances $r = 1, \ldots, 10$ the data were well described by a single exponential, $C(r) \propto \exp(-r/\xi)$. A log-linear fit gave

$$\xi(T = 2.3) = 2.34 \pm 0.05 \tag{45}$$

in lattice units (Fig. 12), much smaller than $L = 32$. A full study of $\xi(T) \sim |T - T_c|^{-\nu}$ would require simulations closer to T_c and is beyond the scope of this project.

7 Algorithmic performance: parallel tempering vs Metropolis

The final part of the project compares the statistical efficiency of parallel tempering with that of a single Metropolis chain at a temperature close to criticality, in terms of autocorrelation times and effective sample sizes.

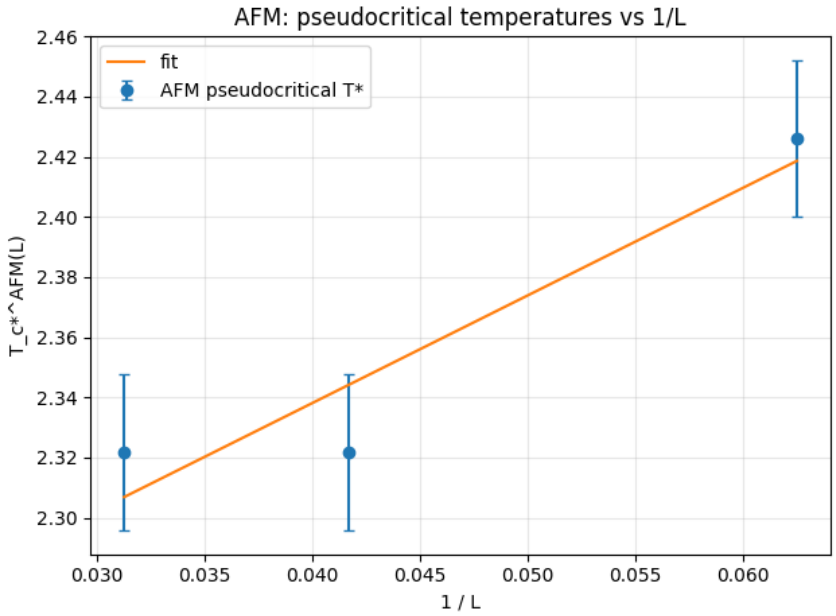

Figure 11: Pseudocritical temperatures $T_c^{*,\mathrm{AFM}}(L)$ from the maxima of the staggered susceptibility plotted against $1/L$.

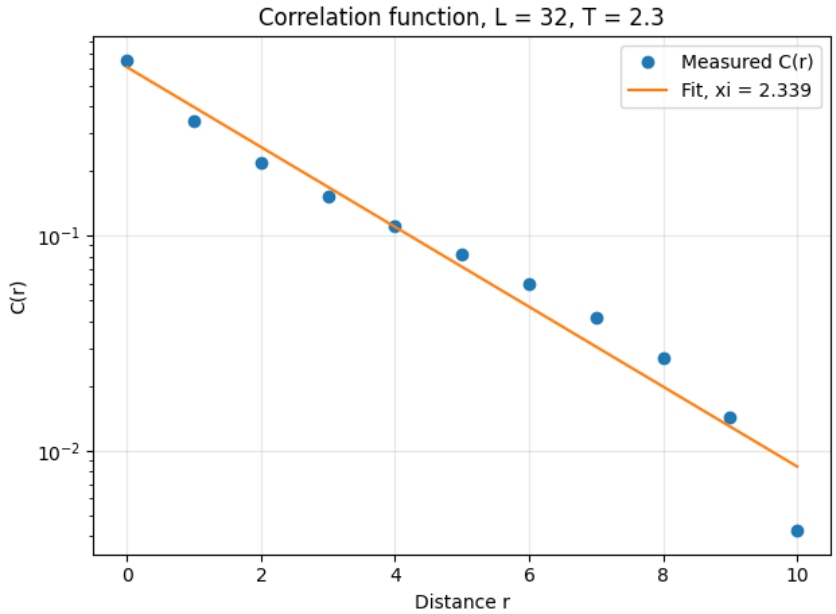

Figure 12: Correlation function for $L = 32$ at $T = 2.3$ with exponential fit, giving $\xi \approx 2.3$ lattice spacings.

7.1 Set-up and summary statistics

PT simulations with $R = 8$ replicas in the range $T \in [1.8, 3.0]$ were run for $L = 16$ and $L = 24$. Each run used 80000 sweeps, of which 20000 were discarded as burn-in, with measurements every 50 sweeps. Swap attempts occurred every 10 sweeps. For each lattice size, a single-temperature Metropolis run at $T = 2.486$ was performed with the same number of sweeps and measurement interval.

For a fair comparison, the energy time series from the PT replica whose temperature was closest to $T = 2.486$ were compared with the single-chain Metropolis time series. The integrated autocorrelation times τ_{int}, effective sample sizes N_{eff} and standard errors of the mean energy are summarised in Table 2.

Table 2: Comparison of parallel tempering and Metropolis for the energy at $T \approx 2.486$.

L	T	τ_{PT}	$N_{\text{eff,PT}}$	SE_{PT}	τ_{Met}	$N_{\text{eff,Met}}$	SE_{Met}	var ratio
16	2.486	0.57	1059	4.99×10^{-3}	0.63	950	5.33×10^{-3}	1.14
24	2.486	0.52	1154	2.94×10^{-3}	0.56	1071	3.15×10^{-3}	1.15

For both lattice sizes PT reduces τ_{int} slightly and increases the effective sample size by about 10–15%. The corresponding reduction in the variance of the mean energy is of the same order, so with the present ladder and system sizes PT is only mildly more efficient than a single Metropolis chain.

7.2 Supporting time-series plots

Figures 13 and 14 show the energy traces for all PT replicas. Replica energies fluctuate over a wide range and show no visible drift. Figure 15 compares the energy traces at $T \approx 2.486$ for $L = 24$ between PT and Metropolis; both explore the same range. Figure 16 compares the corresponding energy histograms, which are statistically indistinguishable.

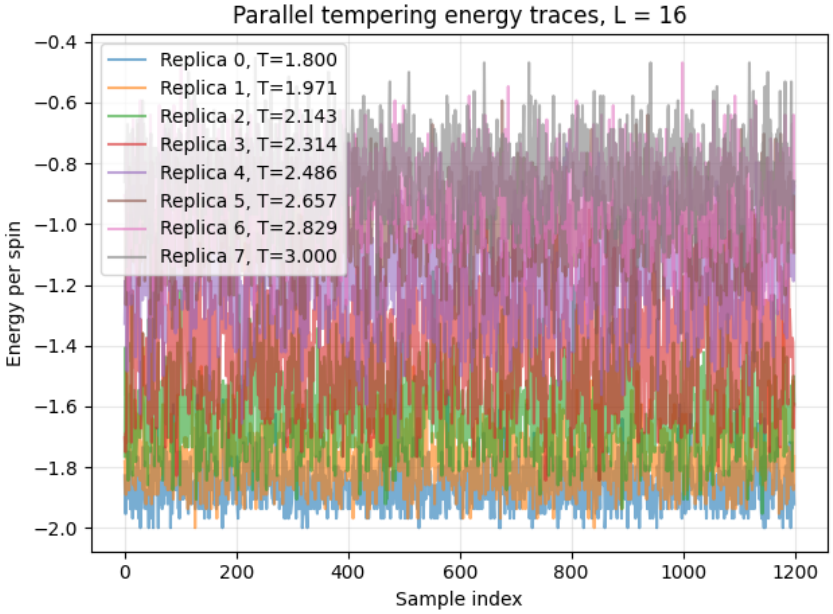

Figure 13: Parallel-tempering energy traces for $L = 16$.

The normalised energy autocorrelation functions in Fig. 17 decay quickly for both algorithms, with PT showing only a slightly faster decay, consistent with the modest difference in τ_{int}.

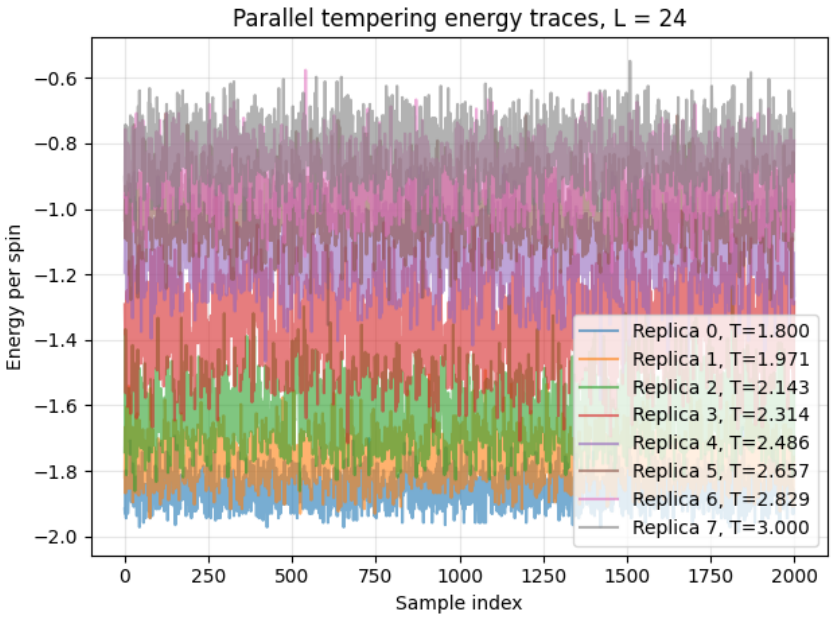

Figure 14: Parallel-tempering energy traces for $L = 24$.

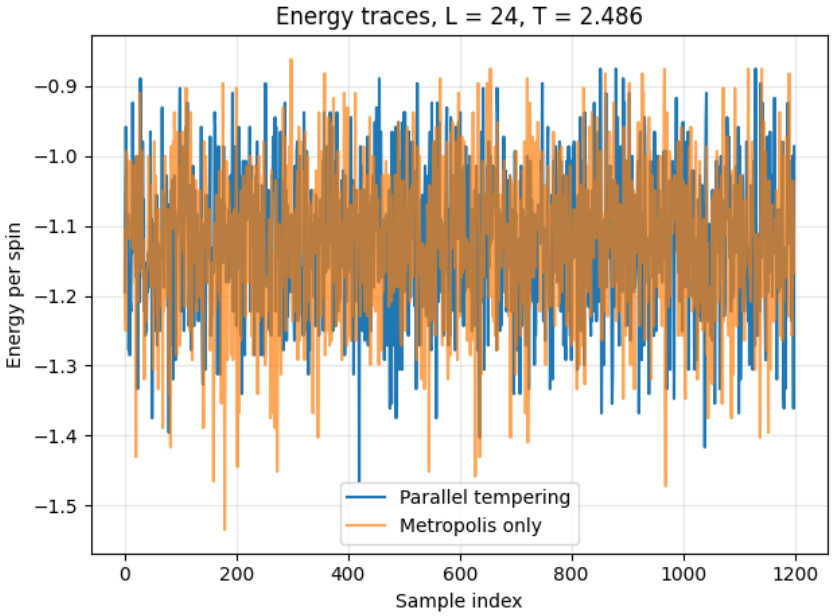

Figure 15: Energy traces at $T \approx 2.486$ for $L = 24$: PT replica versus single Metropolis chain.

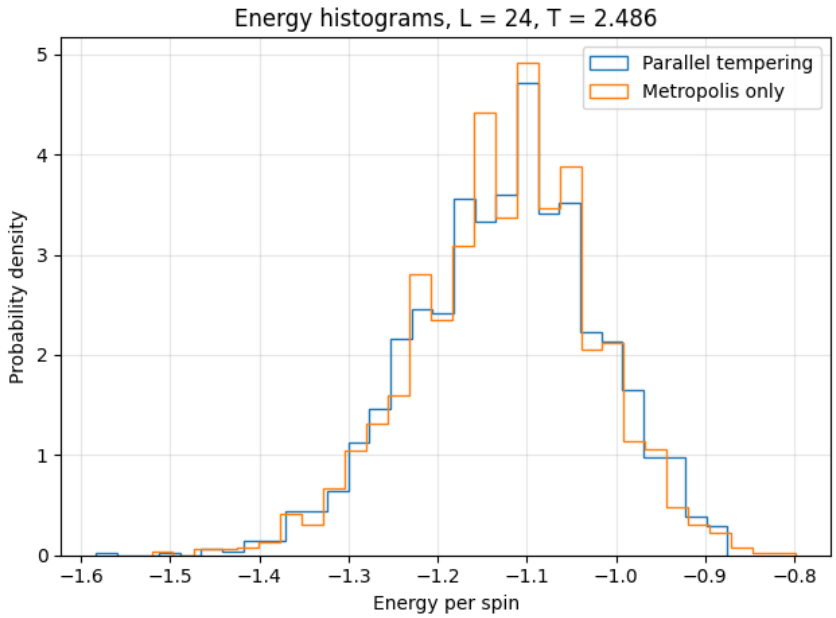

Figure 16: Energy histograms at $T \approx 2.486$ for $L = 24$: PT replica versus Metropolis.

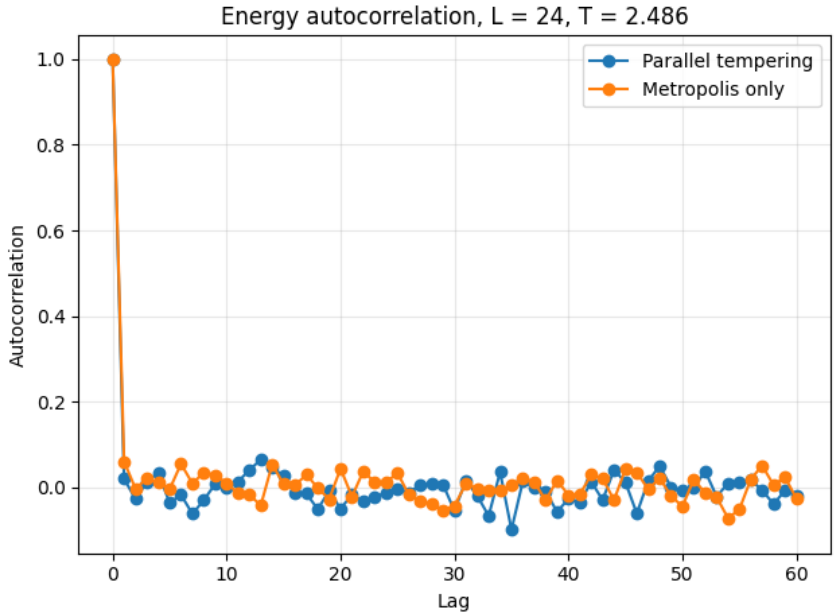

Figure 17: Energy autocorrelation at $T \approx 2.486$ for $L = 24$ for PT and Metropolis.

For the lattice sizes used here, the free-energy barrier between the two magnetised phases is not yet very large, so a local algorithm already explores configuration space reasonably well. PT becomes more advantageous for larger lattices or more strongly metastable systems.

8 Summary and critical assessment

The project combined a simple Monte Carlo integration problem, one- and two-dimensional Ising simulations, finite-size scaling and an algorithmic performance comparison.

For the π estimation problem, 1000 runs with $N = 10000$ samples each produced a distribution of estimates that is very close to a Gaussian. The mean agrees with the true value of π within one standard error, and the measured standard deviation matches the prediction from the central limit theorem, validating the Monte Carlo machinery and error formula used later.

The 1D Ising tests reproduce the exact thermodynamic-limit energy to high accuracy and show a smooth magnetisation curve with no spurious phase transition, confirming that the Metropolis implementation behaves as expected on a model with known analytic results.

For the 2D antiferromagnetic Ising model at $L = 16$, the energy, uniform magnetisation and staggered magnetisation follow the expected pattern: a Néel ordered phase with $\langle |m_s| \rangle \approx 1$ and $\langle |m| \rangle \approx 0$ at low T, and a crossover to a disordered phase around $T \approx 2.3$. A short finite-size scaling analysis of the staggered susceptibility peaks for $L = 16, 24, 32$ gives very noisy estimates $\gamma/\nu_{\mathrm{AFM}} = 1.81 \pm 1.49$ and $T_c^{\mathrm{AFM}}(\infty) = 2.195 \pm 0.054$, which are compatible with the ferromagnetic estimates and Onsager's result but should be interpreted as qualitative checks.

Finite-size scaling of the ferromagnetic susceptibility peaks gives $\gamma/\nu = 1.80 \pm 0.18$, consistent with the exact value $7/4$. The specific-heat peaks are consistent with a weak, logarithmic growth, as expected from $\alpha = 0$. Pseudocritical temperatures extracted from $\chi(T, L)$ give $T_c(\infty) = 2.243 \pm 0.022$, in agreement with the Onsager value within one sigma, and a susceptibility data collapse using these parameters works well. A direct measurement of the correlation function at $T = 2.3$ yields a correlation length $\xi \approx 2.3$ lattice spacings, illustrating how rapidly correlations decay slightly away from T_c.

The parallel-tempering study quantifies the algorithmic gain rather than assuming it: autocorrelation functions, effective sample sizes and standard errors were computed for both PT and Metropolis at two lattice sizes. For the current set-up PT offers only a modest improvement of about 10–15% in the variance of the mean energy.

The main limitations are statistical noise for the largest lattices, the coarse temperature grid and the small number of AFM lattice sizes. Natural extensions would include histogram reweighting to interpolate in temperature and cluster algorithms (such as Wolff or Swendsen–Wang) to reduce critical slowing down near T_c [3, 4]. Within these constraints, the project gives a coherent and quantitatively reasonable picture of the Ising model in one and two dimensions, from simple Monte Carlo integration for π through to critical phenomena and algorithmic performance.

References

[1] L. Onsager, "Crystal statistics. I. A two-dimensional model with an order-disorder transition," *Phys. Rev.* **65**, 117–149 (1944).

[2] R. J. Baxter, *Exactly Solved Models in Statistical Mechanics*, Academic Press, London, 1982.

[3] M. E. J. Newman and G. T. Barkema, *Monte Carlo Methods in Statistical Physics*, Oxford University Press, Oxford, 1999.

[4] D. P. Landau and K. Binder, *A Guide to Monte Carlo Simulations in Statistical Physics*, 4th ed., Cambridge University Press, Cambridge, 2014.

[5] J. Cardy, *Finite-Size Scaling*, North-Holland, Amsterdam, 1988.